J. Phys. B: At. Mol. Phys. 17 (1984) 1427–1444. Printed in Great Britain

Multiple ionisation of multiply charged xenon ions by electron impact

A Müller†, C Achenbach†, E Salzborn† and R Becker‡

† Institut für Kernphysik, Universität Giessen, D-6300 Giessen, West Germany
‡ Institut für Angewandte Physik, Universität Frankfurt, D-6000 Frankfurt, West Germany

Received 12 October 1983

Abstract. Electron–ion crossed beams have been employed to obtain absolute cross sections for double ionisation of Xe^{q+} ions ($q = 1, 2, 3, 4$), threefold ionisation of Xe^{q+} ions ($q = 1, 2, 3$) and fourfold ionisation of Xe^{1+} and Xe^{2+} ions by impact of a single electron with an energy up to 700 eV. Extremely large cross sections have been found showing that multiple ionisation of a complex ion can be as important as single ionisation. The relative strengths of multiple versus single ionisation are investigated as a function of ion charge state, ion atomic number and electron energy. Contributions of inner-shell ionisation are identified.

1. Introduction

In a previous paper we presented absolute electron impact single ionisation cross sections for Xe^{q+} ions ($q = 1, 2, 3, 4$) (Achenbach *et al* 1984). The crossed-beam technique employed was discussed in detail. With the same experimental methods we also measured cross sections for multiple ionisation of multiply charged xenon ions. The data obtained provide detailed information about the relative strengths of multiple versus single electron interactions. The present results show the relevance of multiple ionisation to the charge-state distributions of complex ions in plasmas and imply the necessity of including these processes in plasma modelling calculations.

Multiple ionisation by electron impact has been experimentally studied for atoms for more than fifty years (see e.g. Kieffer 1969, Nagy *et al* 1980, Halle *et al* 1981, Dettmann and Karstensen 1982, Müller *et al* 1983). For ions it was not before 1969 that a direct measurement of cross sections was made: the first experimental cross sections were published for double ionisation of Li^+ ions by Peart and Dolder (1969). A few further measurements followed for double ionisation of H^- ions (Peart *et al* 1971, Defrance *et al* 1982) and multiple ionisation of Rb^+ (Hughes and Feeney 1981) and Cs^+ ions (Hertling *et al* 1982). The first measurements for multiple ionisation of multiply charged ions by electron impact were performed by Müller and Frodl (1980) for Ar^{q+} ions ($q = 1, 2, 3$). Dominant contributions of indirect processes could be identified with ionisation of electrons from the L shell followed by different electron rearrangement processes leading to the ejection of additional electrons. In a recent publication we presented measurements for electron impact double ionisation of I^+ and Xe^{q+} ions ($q = 1, \ldots, 4$) (Achenbach *et al* 1983) and demonstrated the importance of 4d-shell ionisation followed by the ejection of an additional electron. The measured cross sections for I^+ and Xe^+ ions (to a lesser extent also for Xe^{2+}, Xe^{3+} and Xe^{4+}

0022-3700/84/071427+18\$02.25

ions) show a dominant resonance-like contribution which, both in shape and size, almost coincides with the partial 4d photoionisation cross section of Xe atoms. These measurements complement present efforts to understand electron impact ionisation of complex ions and contributed substantially to the clarification of the role of the 4d shell in electron impact ionisation. Pindzola *et al* (1983a) have calculated excitation–autoionisation in the cadmium isoelectronic sequence which exhibits strong target term dependence. Hence measurements of excitation–autoionisation contributions to single ionisation of ions (see Gregory *et al* 1983, Gregory and Crandall 1983, Achenbach *et al* 1984) probe the term dependence in autoionising levels. Studies of multiple ionisation, which may proceed via 4d-shell ionisation (i.e. excitation to the continuum) and the subsequent Auger process, probe the term dependence in the continuum (Pindzola *et al* 1983b). Besides this theoretical interest cross section data for multiple ionisation of ions are also needed for the calibration of ion beam probes used for plasma diagnostics in thermonuclear research reactors (Colestock *et al* 1978). Our results also give a data base for better understanding of multiple ionisation processes relevant in all kinds of plasmas where heavy atoms and ions are present.

2. Experimental technique

The crossed-beam arrangement used for the present experiment has been described in detail by Müller *et al* (1980) and Achenbach *et al* (1984). Absolute cross sections for electron impact multiple ionisation have been determined using the same experimental set-up and the same procedure of data evaluation as in recent experiments by Achenbach *et al.* Here the discussion of the experimental technique can, therefore, be limited.

Beams of multiply charged xenon ions are extracted from an electron beam ion source and accelerated by a voltage of 10 kV. A 90° double focusing magnet selects ions of a given isotope, given charge and energy. A collimated ion beam of about 1.5 mm diameter intersects an intense ribbon-shaped electron beam at an angle of 90°. The electron beam has a perveance of about 10 μA $V^{-3/2}$ and provides an electron current density of 160 mA cm^{-2} at an electron energy of 675 eV extended over 6 cm in the ion beam direction. Thus ionisation rates of the order of 10^{-5} of the incident ion flux are obtained. The residual gas pressure is less than 3×10^{-8} mbar when the electron gun works at full power i.e. 300 W in the electron beam.

Ionised ions are separated by a second 90° magnet from the parent beam and are detected by a single-particle detector which is based on the measurement of secondary electrons released from a converter metal plate by the incident ions (Rinn *et al* 1982). The parent ions are collected by a large Faraday cup inside the magnet chamber.

Electron impact ionisation cross sections σ are determined from

$$\sigma(E)=\frac{S}{I_iI_e}\frac{qe^2v_iv_e}{(v_i^2+v_e^2)^{1/2}}\frac{F}{D} \tag{1}$$

where S is the observed signal count rate, I_i and I_e are the ion and electron beam currents, q is the charge state of the incident ions, e is the charge of an electron, v_i and v_e are the velocities of incident ions and electrons, F is the form factor describing beam overlap and D is the absolute signal detection efficiency. Each of these quantities is carefully determined. The experimental techniques and uncertainties are discussed in the following sections.

2.1. *Ionisation signal and background*

Ionisation signal S and background B are separated by moving the operating electron gun out of the ion beam line without switching off the electron beam. Thus gas desorption from the anode by incident electrons which can cause an additional background by ion stripping is correctly taken into account if the background does not change with the position of the electron gun. The electron gun is an open structure which can be well pumped and does not retain the desorbed gas. By a charge transfer reaction with the electron beam 'in' and 'out' we have checked that the background count rate is the same in both positions within $\pm 5\%$. In the experiments with multiple ionisation of xenon ions very low background count rates were observed. B never exceeded $20\ \mathrm{s}^{-1}$ and was in most cases less than $10\ \mathrm{s}^{-1}$.

This seems to be due to the small multiple-stripping cross sections of xenon ions in the residual gas and at the collimating apertures. Therefore we found very high ratios of signal and background with S/B up to 2000. Hence the relative uncertainty in signal determination ($\Delta S/S$) due to the uncertain determination of the background ($\Delta B/B \leq 0.05$) is negligible for the cross section measurements.

The absolute ionisation rate is given by $R = S/D$. The detector efficiency D is uniform over the entrance aperture (2 cm diameter) of the single-particle detector and equals 0.95 ± 0.03 (Rinn *et al* 1982). We have assured complete transmission of product and parent ion beams by measurement of ion currents in three different Faraday cups just behind the interaction region, within the magnet chamber and in front of the single-particle detector behind the second analysing magnet. By the employment of iris apertures behind the electron gun where the ion beam emerges from the electron beam and in front of the single-particle detector the maximum diameter of parent and product ion beams can be determined. The measurements showed that both beams are narrow compared with the beam-limiting apertures. Especially the height of the magnet chamber is comparatively large: 3 cm. With a beam divergence of less than 0.25° determined by a collimator in front of the ion beam (two apertures with 0.5 mm diameter each, 230 mm apart) the ion beams reach at most 5 mm diameter.

Correct determination of the background is assured by vanishing cross sections below the ionisation threshold (see figures 1 and 2). The fact that no signal was obtained below threshold also indicates that highly excited metastable ions in the incident beam do not play a role. Also, a possible background due to trapping of slow residual gas ions in the electron beam can, therefore, be ruled out. A detailed discussion of this possible source of error was given in our previous paper (Achenbach *et al* 1984).

2.2. *Electron energy and form factor*

The electron gun used in this experiment was designed for exceptionally high ionisation efficiency which by far exceeds that of common crossed-beam experiments. The electric potential distribution and the resulting electron trajectories were calculated and optimised by using a computer code which solves the Poisson equation for a given geometry and the equations of motion for the electrons. The electron space charge is taken into account as well as the velocity distribution of electrons thermally emitted by the cathode (Sinz 1981, Achenbach *et al* 1984).

The geometry and applied electric potentials were chosen such that the incident ion beam is not deflected or focused as long as it crosses within a definite area around the required position of the ion beam axis. Within this area which resembles a tube of 3 mm × 3 mm along the ion beam axis the electric potential is uniform with deviations of less than 0.3%. Thus the definition of the electron energy is uncertain to ±3 eV in the worst case, i.e. for a voltage of $U_{CA} = 1000$ V between cathode and anode. According to the calculation the electron energy in the region of the intersecting beam is $0.675eU_{CA}$ which was experimentally confirmed by the observed thresholds of the investigated ionisation processes. Within the volume where the electric potential is constant the electron current density is also uniform with deviations of less than ±5%. This was experimentally confirmed by scanning the area with a very narrow ion beam (0.2 mm diameter collimators) and observing the ionisation signal which did not change by more than ±5%. We also used ion beams of different diameters and found constant ratios of S/I_i (see equation (1)) as long as the beam diameter did not exceed 3 mm. When the electron current density j_e is constant within the interaction region the form factor F reduces to

$$F = I_e/(b_e j_e) \tag{2}$$

where b_e is the width of the electron beam in the ion beam direction ($b_e = 6$ cm). Because of the sophisticated design of the electron gun it is difficult, however, to measure the electron current density directly. A metal scanner for probing the electron beam current density might change the potentials inside the beam and thus lead to errors. We decided therefore to determine j_e by comparison of apparent cross sections with known data from the literature. For this purpose we remeasured cross sections $\sigma_{1,2}$ for single ionisation of Ar^+ ions and compared our results with experimental values obtained by Woodruff *et al* (1978), since a low absolute uncertainty is claimed for their measurements. By the comparison we found

$$j_e b_e/I_e = 1/F = (-0.483 + 1.256 \lg U_{CA}/V)\ \mathrm{cm}^{-1} \tag{3}$$

with a relative uncertainty $\Delta F/F$ of typically 4% which has to be combined with the absolute uncertainty of the data used for normalisation (less than ±10%).

2.3. *Uncertainties*

The main uncertainties inherent in the present measurements have been discussed above. Because of the high ionisation efficiency of the electron beam we can easily obtain such a number of counts for the signal with and without the electron beam in the ion beam line that the purely statistical error is less than ±1% at a 95% confidence level. Only in the very threshold region higher counting errors may occur due to the vanishing cross section.

The uncertainties of the cross section measurements are listed in table 1.

The typical total uncertainty at good confidence is obtained as the quadrature sum of the individual uncertainties arising from the sources which are listed in table 1.

The measured cross section data are listed in table 2. The errors given combine the statistical error of counting and the error in the determination of the form factor F due to the random scatter in the remeasurement of $\sigma_{1,2}$ for Ar^+ ions.

We also include the numerical values of cross sections for double ionisation of multiply charged xenon ions and I^+ ions which were published in the previous paper (Achenbach *et al* 1983).

Table 1. Experimental uncertainties.

Source	Uncertainty (%)
(*a*) Cross section $\sigma_{q,q+k}$ $(k=2,3,4)$	
Counting statistics (typical value above ionisation threshold at 95% confidence limit)	±1
Form factor F (relative uncertainty of $j_e b_e/I_e$	±4
Additional systematic undertainties	
Counting efficiency	±3
Ion current I_i	±2
Electron current I_e	±2
Ion velocity v_i	±1
Absolute uncertainty of F due to normalisation to data of Woodruff *et al* (1978)	±5 to ±9
Quadrature sum	±7.7 to ±10.8
(*b*) Electron energy E	
Measurement of the potential U_{CA}	±3
Uncertainty of calculated electron energy (est)	±0.2

Table 2. Multiple ionisation cross sections by electron impact. Only relative uncertainties are given.

	Electron energy (eV)	Cross section (10^{-17} cm^2)	Electron energy (eV)	Cross section (10^{-17} cm^2)
$\sigma_{1,3}$	40.5	0.04±0.03	195.8	3.26±0.13
$Xe^+ \to Xe^{3+}$	47.3	0.04±0.03	202.5	3.23±0.13
	50.6	0.01±0.01	216.0	3.07±0.13
	54.0	0.13±0.01	222.8	3.12±0.13
	57.4	0.39±0.07	229.5	3.04±0.12
	60.8	0.60±0.03	236.3	3.05±0.12
	67.5	0.94±0.04	243.0	3.00±0.12
	74.3	1.39±0.06	249.8	3.04±0.12
	81.0	2.17±0.09	253.1	3.02±0.12
	87.8	3.06±0.12	256.6	2.98±0.12
	94.5	3.92±0.16	263.3	2.98±0.12
	101.3	4.51±0.18	270.0	2.98±0.12
	108.0	4.86±0.20	270.0	2.98±0.12
	114.8	5.02±0.20	286.9	2.94±0.12
	118.1	4.83±0.19	297.0	2.97±0.12
	121.5	4.93±0.20	303.8	2.94±0.12
	128.3	4.74±0.19	320.8	2.94±0.12
	135.0	4.45±0.18	337.5	2.88±0.12
	141.8	4.52±0.18	344.3	2.84±0.11
	148.5	4.04±0.16	354.4	2.83±0.11
	151.9	3.94±0.16	371.3	2.82±0.11
	155.3	3.85±0.16	388.1	2.78±0.11
	162.0	3.71±0.15	405.0	2.68±0.11
	168.8	3.62±0.15	405.0	2.79±0.11
	175.5	3.52±0.14	411.8	2.75±0.11
	182.3	3.45±0.14	421.9	2.65±0.11
	185.5	3.41±0.14	432.0	2.68±0.11
	189.0	3.33±0.13	438.8	2.59±0.10

Table 2. (continued)

	Electron energy (eV)	Cross section (10^{-17} cm^2)	Electron energy (eV)	Cross section (10^{-17} cm^2)
	452.3	2.66±0.11	573.8	2.29±0.09
	455.6	2.56±0.10	590.6	2.26±0.09
	465.8	2.63±0.11	590.6	2.40±0.10
	472.5	2.53±0.10	607.5	2.28±0.09
	489.4	2.58±0.10	624.4	2.21±0.09
	506.3	2.45±0.10	624.4	2.33±0.09
	523.1	2.47±0.10	641.3	2.22±0.09
	540.0	2.38±0.10	658.1	2.30±0.09
	556.9	2.45±0.10	675.0	2.07±0.08
$\sigma_{2,4}$	40.5	0.00	205.9	2.90±0.12
$Xe^{2+} \rightarrow Xe^{4+}$	67.5	0.01±0.02	209.3	2.83±0.12
	74.3	0.20±0.02	216.0	2.82±0.12
	77.6	0.49±0.03	216.0	2.80±0.11
	81.0	0.95±0.05	219.4	2.84±0.12
	84.4	1.31±0.06	222.8	2.81±0.11
	87.8	1.59±0.07	222.8	2.91±0.12
	91.1	1.96±0.09	229.5	2.85±0.12
	94.5	2.23±0.10	229.5	2.79±0.11
	97.9	2.57±0.11	232.9	2.85±0.12
	101.3	2.70±0.12	236.3	2.79±0.11
	104.6	2.91±0.12	243.0	2.80±0.11
	108.0	3.14±0.14	243.0	2.86±0.12
	111.4	3.17±0.13	246.4	2.81±0.11
	114.8	3.34±0.15	249.8	2.89±0.12
	118.1	3.31±0.13	256.5	2.75±0.11
	121.5	3.34±0.15	256.5	2.87±0.12
	124.9	3.38±0.14	259.9	2.82±0.12
	128.3	3.47±0.15	270.0	2.88±0.12
	131.6	3.37±0.14	270.0	2.78±0.11
	135.0	3.37±0.14	273.4	2.83±0.12
	135.0	3.43±0.15	276.8	2.88±0.12
	138.4	3.32±0.14	280.1	2.80±0.11
	141.8	3.49±0.14	286.9	2.77±0.11
	145.1	3.32±0.14	286.9	2.87±0.12
	148.5	3.32±0.15	293.6	2.79±0.11
	151.9	3.25±0.13	303.8	2.86±0.12
	151.9	3.27±0.13	310.5	2.85±0.12
	158.6	3.25±0.13	313.9	2.78±0.11
	162.0	3.35±0.14	320.6	2.82±0.11
	165.4	3.23±0.13	334.1	2.76±0.11
	168.8	3.26±0.14	337.5	2.80±0.11
	168.8	3.33±0.14	354.4	2.79±0.11
	175.5	3.28±0.14	357.8	2.69±0.11
	178.9	3.11±0.13	371.3	2.74±0.11
	182.3	3.08±0.13	378.0	2.65±0.11
	189.0	3.09±0.13	388.1	2.70±0.11
	192.4	2.98±0.12	398.3	2.76±0.11
	195.8	3.03±0.12	405.0	2.70±0.11
	195.8	2.90±0.12	421.9	2.69±0.11
	202.5	2.90±0.12	425.3	2.74±0.11

Table 2. (continued)

	Electron energy (eV)	Cross section (10^{-17} cm^2)	Electron energy (eV)	Cross section (10^{-17} cm^2)
	438.8	2.62±0.11	556.9	2.47±0.10
	452.3	2.71±0.11	573.8	2.37±0.10
	455.6	2.57±0.10	607.5	2.32±0.09
	472.5	2.58±0.10	624.4	2.41±0.10
	489.4	2.60±0.10	641.3	2.28±0.09
	492.8	2.52±0.10	658.1	2.29±0.09
	513.0	2.50±0.10	675.0	2.24±0.09
	540.0	2.40±0.10		
$\sigma_{3,5}$	81.0	0.01±0.03	216.0	2.15±0.09
$Xe^{3+} \rightarrow Xe^{5+}$	94.5	0.06±0.04	229.5	2.11±0.09
	97.9	0.12±0.05	243.0	2.11±0.09
	101.3	0.31±0.04	256.5	2.07±0.09
	104.6	0.50±0.05	270.0	2.11±0.09
	108.0	0.74±0.06	276.8	2.10±0.09
	111.4	0.93±0.06	286.9	2.05±0.09
	114.8	1.11±0.07	303.8	2.08±0.09
	118.1	1.28±0.07	320.6	2.05±0.08
	121.5	1.33±0.07	337.5	2.06±0.08
	124.9	1.52±0.08	354.4	2.00±0.08
	128.3	1.58±0.08	371.3	2.01±0.08
	131.6	1.61±0.08	388.1	1.96±0.08
	135.0	1.71±0.08	405.0	1.98±0.08
	138.4	1.81±0.09	421.9	1.93±0.08
	141.8	1.91±0.09	438.8	1.89±0.08
	148.5	2.01±0.09	455.6	1.91±0.08
	155.3	2.19±0.10	472.5	1.89±0.08
	162.0	2.26±0.10	492.8	1.88±0.08
	168.8	2.33±0.10	513.0	1.81±0.07
	175.5	2.34±0.10	540.0	1.79±0.07
	182.3	2.25±0.10	573.8	1.73±0.07
	189.0	2.25±0.10	607.5	1.70±0.07
	195.8	2.22±0.10	641.3	1.66±0.07
	202.5	2.21±0.10	675.0	1.63±0.07
$\sigma_{4,6}$	101.3	0.023±0.04	249.8	1.01±0.05
$Xe^{4+} \rightarrow Xe^{6+}$	118.1	0.046±0.04	256.5	1.01±0.05
	128.3	0.192±0.026	263.3	1.02±0.05
	135.0	0.328±0.034	270.0	1.01±0.05
	148.5	0.625±0.037	283.5	0.964±0.042
	162.0	0.816±0.044	297.0	0.954±0.041
	168.8	0.987±0.054	303.8	0.932±0.042
	175.5	1.02±0.05	320.6	0.945±0.040
	189.0	1.05±0.05	337.5	0.922±0.041
	202.5	1.10±0.05	354.4	0.907±0.038
	209.3	1.04±0.05	371.3	0.899±0.039
	216.0	1.11±0.05	388.1	0.874±0.037
	229.5	1.07±0.05	405.0	0.881±0.038
	236.3	1.05±0.05	421.9	0.882±0.037
	243.0	1.07±0.05	428.8	0.836±0.036

Table 2. (continued)

	Electron energy (eV)	Cross section (10^{-17} cm^2)	Electron energy (eV)	Cross section (10^{-17} cm^2)
	455.6	0.830±0.035	573.8	0.733±0.032
	472.5	0.829±0.036	607.5	0.728±0.031
	489.4	0.798±0.034	641.3	0.694±0.030
	506.3	0.783±0.031	675.0	0.680±0.029
	540.0	0.761±0.033		
$\sigma_{1,3}$	40.5	0.00±0.00	195.8	3.56±0.14
$I^+ \rightarrow I^{3+}$	47.3	0.04±0.03	202.5	3.54±0.14
	50.6	0.11±0.02	209.3	3.57±0.14
	54.0	0.37±0.02	216.0	3.48±0.14
	57.4	0.58±0.03	229.5	3.48±0.14
	60.8	0.79±0.04	243.0	3.43±0.14
	64.1	1.03±0.05	256.5	3.40±0.14
	67.5	1.39±0.06	263.3	3.42±0.14
	67.5	1.34±0.06	270.0	3.38±0.14
	69.5	1.64±0.08	283.5	3.36±0.14
	70.9	1.74±0.08	297.0	3.36±0.14
	74.3	2.12±0.09	310.5	3.31±0.13
	77.6	2.54±0.11	324.0	3.29±0.13
	81.0	3.01±0.13	330.8	3.27±0.13
	84.4	3.39±0.14	337.5	3.19±0.13
	87.8	3.77±0.16	354.4	3.22±0.13
	94.5	4.34±0.18	371.3	3.10±0.13
	101.3	4.76±0.20	388.1	3.11±0.13
	108.0	4.95±0.20	394.4	3.09±0.12
	111.4	5.14±0.21	405.0	3.02±0.12
	114.8	5.10±0.21	425.3	3.00±0.12
	121.5	5.03±0.21	445.5	2.95±0.12
	128.3	4.91±0.20	455.6	2.91±0.12
	131.6	4.92±0.20	465.8	2.89±0.12
	135.0	4.67±0.19	486.0	2.85±0.11
	141.8	4.49±0.18	506.3	2.80±0.11
	148.5	4.27±0.17	523.1	2.77±0.11
	151.9	4.26±0.17	540.0	2.73±0.11
	155.3	4.15±0.17	556.9	2.73±0.11
	162.0	4.03±0.16	573.8	2.70±0.11
	168.8	3.90±0.16	607.5	2.64±0.11
	175.5	3.75±0.15	641.3	2.57±0.10
	182.3	3.71±0.15	675.0	2.53±0.10
	189.0	3.63±0.15		
$\sigma_{1,4}$	87.8	0.001±0.002	155.3	0.773±0.032
$Xe^+ \rightarrow Xe^{4+}$	94.5	0.001±0.001	162.8	0.841±0.034
	97.9	0.011±0.003	168.8	0.901±0.037
	101.3	0.046±0.003	168.8	0.898±0.038
	108.0	0.136±0.007	182.3	0.963±0.039
	114.8	0.270±0.012	189.0	0.996±0.040
	121.5	0.398±0.017	195.8	0.987±0.040
	128.3	0.508±0.021	202.5	0.990±0.040
	135.0	0.594±0.025	209.3	0.985±0.040
	141.8	0.662±0.027	216.0	0.961±0.039
	148.5	0.713±0.029	229.5	0.926±0.037

Table 2. (continued)

	Electron energy (eV)	Cross section (10^{-17} cm^2)	Electron energy (eV)	Cross section (10^{-17} cm^2)
	236.3	0.931 ± 0.037	418.5	0.743 ± 0.030
	243.0	0.898 ± 0.036	432.0	0.735 ± 0.030
	256.5	0.870 ± 0.035	452.3	0.703 ± 0.028
	270.0	0.843 ± 0.034	465.8	0.708 ± 0.028
	276.8	0.853 ± 0.034	472.5	0.698 ± 0.028
	283.5	0.872 ± 0.035	472.5	0.673 ± 0.027
	286.9	0.810 ± 0.033	489.4	0.681 ± 0.027
	297.0	0.850 ± 0.034	506.3	0.667 ± 0.027
	303.8	0.800 ± 0.032	523.1	0.651 ± 0.026
	317.3	0.840 ± 0.034	540.0	0.637 ± 0.026
	320.6	0.794 ± 0.032	556.9	0.623 ± 0.025
	330.8	0.827 ± 0.033	573.8	0.619 ± 0.025
	344.3	0.804 ± 0.032	590.6	0.604 ± 0.024
	344.3	0.787 ± 0.032	607.5	0.610 ± 0.025
	357.8	0.794 ± 0.032	624.4	0.594 ± 0.024
	378.0	0.778 ± 0.031	641.3	0.579 ± 0.023
	391.5	0.757 ± 0.030	658.1	0.558 ± 0.022
	398.3	0.758 ± 0.030	675.0	0.556 ± 0.022
	411.8	0.741 ± 0.030		
$\sigma_{2,5}$	67.5	−0.001 ± 0.007	293.6	0.585 ± 0.024
$Xe^{2+} \to Xe^{5+}$	87.8	−0.015 ± 0.02	303.8	0.586 ± 0.024
	101.3	−0.000 ± 0.001	320.6	0.578 ± 0.024
	128.3	0.004 ± 0.003	327.4	0.560 ± 0.023
	141.8	0.061 ± 0.004	337.5	0.551 ± 0.022
	148.5	0.105 ± 0.006	354.4	0.545 ± 0.022
	155.3	0.162 ± 0.008	371.3	0.537 ± 0.022
	162.0	0.244 ± 0.011	388.1	0.537 ± 0.022
	168.8	0.309 ± 0.013	405.0	0.535 ± 0.022
	175.5	0.392 ± 0.017	411.8	0.526 ± 0.021
	182.3	0.469 ± 0.020	421.9	0.530 ± 0.021
	189.0	0.520 ± 0.022	438.8	0.508 ± 0.021
	195.8	0.563 ± 0.023	445.5	0.517 ± 0.021
	202.5	0.603 ± 0.025	455.6	0.494 ± 0.020
	209.3	0.614 ± 0.025	472.5	0.510 ± 0.021
	216.0	0.631 ± 0.026	479.3	0.485 ± 0.020
	222.8	0.636 ± 0.026	492.8	0.504 ± 0.020
	229.5	0.653 ± 0.027	513.0	0.468 ± 0.019
	236.3	0.633 ± 0.026	540.0	0.458 ± 0.018
	243.0	0.642 ± 0.026	550.1	0.450 ± 0.018
	249.8	0.631 ± 0.026	573.8	0.438 ± 0.018
	256.5	0.630 ± 0.026	573.8	0.619 ± 0.018
	270.0	0.619 ± 0.025	607.5	0.430 ± 0.017
	280.1	0.598 ± 0.025	641.3	0.416 ± 0.016
	286.9	0.593 ± 0.024	675.0	0.399 ± 0.016
$\sigma_{3,6}$	135.0	0.053 ± 0.02	192.4	0.131 ± 0.012
$Xe^{3+} \to Xe^{6+}$	155.3	0.040 ± 0.010	202.5	0.209 ± 0.014
	168.8	0.034 ± 0.012	209.3	0.214 ± 0.015
	175.5	0.028 ± 0.011	216.0	0.234 ± 0.013
	185.6	0.099 ± 0.010	226.1	0.271 ± 0.015

Table 2. (continued)

	Electron energy (eV)	Cross section (10^{-17} cm^2)	Electron energy (eV)	Cross section (10^{-17} cm^2)
	236.3	0.323±0.017	405.0	0.363±0.016
	246.4	0.309±0.016	421.9	0.344±0.015
	253.1	0.335±0.017	438.8	0.350±0.015
	259.9	0.339±0.017	455.6	0.344±0.014
	270.0	0.364±0.018	472.5	0.364±0.016
	286.9	0.362±0.017	506.3	0.331±0.014
	303.8	0.359±0.017	540.0	0.333±0.014
	337.5	0.361±0.016	573.8	0.313±0.013
	354.4	0.351±0.016	573.8	0.306±0.013
	371.3	0.357±0.017	641.3	0.303±0.013
	388.1	0.343±0.015	675.0	0.301±0.013
$\sigma_{1,5}$ $Xe^{+} \rightarrow Xe^{5+}$	135.0	0.001±0.002	337.5	0.280±0.011
	141.8	0.001±0.001	354.4	0.278±0.011
	148.5	0.003±0.001	357.8	0.280±0.011
	155.3	0.003±0.001	371.3	0.279±0.011
	162.0	0.007±0.001	378.0	0.284±0.011
	168.8	0.019±0.001	405.0	0.281±0.011
	175.5	0.036±0.002	411.8	0.287±0.012
	182.3	0.057±0.003	421.9	0.278±0.011
	189.0	0.084±0.004	438.8	0.279±0.011
	195.8	0.109±0.005	455.6	0.279±0.011
	202.5	0.138±0.006	459.0	0.285±0.011
	209.3	0.162±0.007	472.5	0.286±0.011
	216.0	0.183±0.008	472.5	0.278±0.011
	222.8	0.202±0.008	489.4	0.285±0.011
	229.5	0.223±0.009	506.3	0.269±0.011
	236.3	0.236±0.010	506.3	0.279±0.011
	243.0	0.250±0.010	523.1	0.277±0.011
	249.8	0.254±0.011	540.0	0.268±0.011
	256.5	0.265±0.011	540.0	0.272±0.011
	263.3	0.273±0.011	556.9	0.258±0.010
	270.0	0.278±0.011	573.8	0.239±0.010
	273.4	0.284±0.012	573.8	0.260±0.010
	283.5	0.285±0.011	590.6	0.264±0.011
	286.9	0.286±0.011	607.5	0.248±0.010
	297.0	0.285±0.011	607.5	0.266±0.011
	303.8	0.282±0.011	641.3	0.242±0.010
	307.1	0.288±0.011	641.3	0.262±0.011
	310.5	0.284±0.011	658.1	0.239±0.010
	317.3	0.278±0.011	675.0	0.243±0.010
	327.4	0.278±0.011	675.0	0.224±0.009
	330.8	0.286±0.011		
$\sigma_{2,6}$ $Xe^{2+} \rightarrow Xe^{6+}$	135.0	0.002±0.001	253.1	0.053±0.003
	175.5	0.006±0.001	270.0	0.074±0.003
	189.0	0.004±0.001	286.9	0.091±0.004
	202.5	0.007±0.001	303.8	0.103±0.004
	219.4	0.016±0.001	320.6	0.111±0.005
	236.3	0.038±0.002	337.5	0.111±0.005

Table 2. (continued)

Electron energy (eV)	Cross section (10^{-17} cm^2)	Electron energy (eV)	Cross section (10^{-17} cm^2)
371.3	0.119 ± 0.005	540.0	0.110 ± 0.005
405.0	0.122 ± 0.005	573.8	0.100 ± 0.004
438.8	0.116 ± 0.005	607.5	0.106 ± 0.004
472.5	0.117 ± 0.005	641.3	0.103 ± 0.004
506.3	0.115 ± 0.005	675.0	0.096 ± 0.004

3. Results and discussion

3.1. Double ionisation

In a recent paper we have already presented our results for electron impact double ionisation of Xe^{q+} ions ($q = 1, 2, 3, 4$) and I^+ ions (Achenbach *et al* 1983). We demonstrated the importance of a two-step mechanism involving single ionisation of the 4d subshell and subsequent autoionisation. Unexpectedly, the cross section $\sigma^{4d}_{q,q+2}$ assigned to this indirect process nearly coincides, both in shape and size, with the partial 4d-shell photoionisation cross section of Xe atoms.

There is no general theoretical concept available to calculate multiple ionisation cross sections for electrons incident on ions. Only for the direct ejection of two electrons from an atom or ion Gryzinski (1965) has developed a classical picture in which either the incident fast electron may hit two target electrons in successive collisions or the fast electron knocks out one target electron which is energetic enough to eject another target electron during its passage out of the electron cloud. From this concept a rough estimate for the direct double-knock-out cross section may be obtained. Also the single ionisation of the 4d shell is a direct ionisation process for which a cross section can be calculated from the well known and often used formula of Lotz (1968). Figure 1 shows a comparison of the total electron impact double-ionisation cross section calculated as a sum of the two contributions (Gryzinski and Lotz) with our measurements for Xe^+ ions. Obviously there is a large discrepancy around $E_e \simeq 100$ eV. The resonance-like peak which we previously could attribute to 4d-shell ionisation has a shape which is completely different from all that can be expected on the basis of simple theories which do not include the many-body character of the electronic interactions involved.

Distorted-wave calculations for many-electron ions have demonstrated a pronounced sensitivity of the ionisation cross section to the description of the low-energy final-state electron (Younger 1982). The problem of one continuum electron outside a complex target has been extensively studied in photoionisation work especially also in the case of opening a closed nd subshell (see e.g. Cooper 1964, Ederer 1964, Lucatorto *et al* 1981).

Effects of collapsing wavefunctions, which may be very sensitive to small changes in the core orbitals, electron correlations, term dependence and autoionisation have been identified to determine the size and shape of photoionisation cross sections. Obviously atomic structure effects also can dramatically change the expected cross

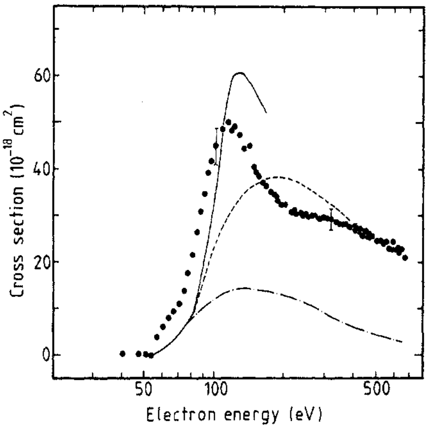

Figure 1. Comparison of the measured double-ionisation cross section for Xe^+ ions with DW calculations of Pindzola *et al* (——), with calculations of Gryzinski for direct double ionisation (— · —) and with the sum of the Lotz 4d contribution and Gryzinski direct double ionisation contribution (- - -).

sections for electron impact ionisation. Pindzola *et al* (1983b) have made calculations for the ionisation of a 4d electron from a Xe^+ ion by either a photon or an electron. For photoionisation they found a dramatic change in the calculated cross section by including term dependence in the continuum. By the inclusion of pair correlations in the ground state of Xe they could reproduce the experimental 4d photoionisation cross section for Xe atoms well. In order to interpret our Xe^+ double-ionisation experiment, they made distorted-wave electron impact ionisation cross section calculations similar in spirit to those of Younger (1980, 1982). The term-dependent Hartree–Fock calculation with ground-state correlations gives a fair representation of the experimental data. Especially the unusual shape of the 4d contribution to double-electron impact ionisation of Xe^+ ions is well reproduced. The calculations of Pindzola *et al* are also shown in figure 1.

3.2. Triple and quadruple ionisation

Figure 2 shows measured cross sections for triple ionisation of Xe^{q+} ions $\sigma_{q,q+3}$ with $q = 1, 2, 3$ and for quadruple ionisation of Xe^{q+} ions $\sigma_{q,q+4}$ with $q = 1, 2$. These cross sections are extremely large compared with known data for ions: The maximum of $\sigma_{1,5}$ in the present energy range, with a value of 3×10^{-18} cm^2 for Xe^+ is about 60 times higher than that for Ar^+ ions measured by Müller and Frodl (1980). This comparison shows the importance of multiple ionisation processes for a many-electron ion. As discussed in the previous section indirect ionisation processes are relevant and may by far dominate the direct ejection of several outer electrons. In contrast to the case of Ar^{q+} ions multiple ionisation of Xe^{q+} ions is much more complex since there is no longer such a pronounced energetic separation of the different electron shells. The shells involved in the investigated electron energy range are the $n = 5$ ($5s^2$, $5p^{6-q}$) and the $n = 4$ ($4s^2$, $4p^6$, $4d^{10}$) subshells. As a consequence it is energetically possible to eject more than one inner-shell electron or to excite the ion into a highly excited bound state with subsequent multiple autoionisation. The number of subshells involved at a given energy is increased and an analysis of the experimental data on the basis of

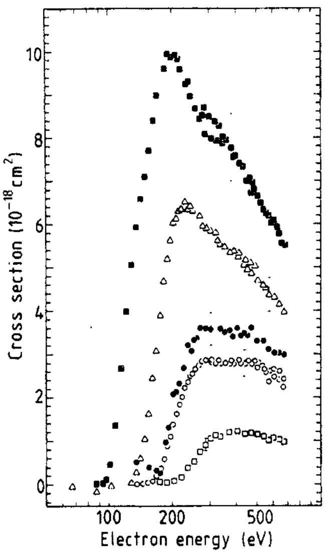

Figure 2. Cross sections for the threefold and fourfold ionisation of Xe^{q+} ions. $\sigma_{q,q+3}$: $e+Xe^{q+} \rightarrow Xe^{(q+3)+}+4e$ ($q=1,2,3$); $\sigma_{q,q+4}$: $e+Xe^{q+} \rightarrow Xe^{(q+4)+}+5e$ ($q=1,2$). $\sigma_{1,4}$: ■; $\sigma_{1,5}$: ○; $\sigma_{2,5}$: △; $\sigma_{2,6}$: □; $\sigma_{3,6}$: ●. For threefold ionisation of Xe^{3+} the cross sections $\sigma_{3,6}$ at 135 and 155.3 eV appear to be non-zero below threshold. These results reflect the difficulties in cross section determination at and below threshold when the ratio of signal to background S/B is small or zero (see discussion in § 2.1).

energetically allowed processes which could be performed for Ar^{q+} ions becomes too complex for the present Xe^{q+} ions.

Also, the data for triple and quadruple ionisation do not show unambiguous threshold steps which could be used as fingerprints of special ionisation mechanisms as in the case of the 4d contribution to double ionisation. It is remarkable that the cross sections $\sigma_{3,6}$, $\sigma_{1,5}$ and $\sigma_{2,6}$ are rather flat for electron energies above 300 eV, which is certainly a hint for increasing relative contributions of indirect processes. We should also mention that the thresholds of all ionisation cross sections measured are compatible with the single-ionisation energies $I_{1,2}=21.2$ eV for Xe^+, $I_{2,3}=32.1$ eV for Xe^{2+}, $I_{3,4}=43$ eV for Xe^{3+}, $I_{4,5}=55$ eV for Xe^{4+} and $I_{5,6}=67$ eV for Xe^{5+} ions: non-zero cross sections are measured beginning from the minimum electron energy

$$I_{q,q+k} = \sum_{j=q}^{q+k-1} I_{j,j+1}$$

that is needed to eject the k outermost electrons.

3.3. *Relative strengths of multiple versus single ionisation*

Multiple ionisation of *atoms* by electron impact has received continuous interest since the beginning of experimental atomic collision physics. Early work has been reviewed by Kieffer and Dunn (1966). Ratios of multiple to single ionisation of atoms have been measured at different electron energies especially for the rare gases (Schram *et al* 1966, Schram 1966, El-Sherbini *et al* 1970, Nagy *et al* 1980, Müller *et al* 1983) the alkali atoms and the earth-alkali atoms (Kieffer 1969, Dettman and Karstensen 1982). With the electron energy increasing beyond the respective ionisation threshold these ratios increase and then tend to become constant. For example, the ratio $R_2^{(0)} = \sigma_{0,2}/\sigma_{0,1}$ for He atoms is 2.66×10^{-3} at 16 keV (Schram *et al* 1966) and 2.6×10^{-3} at 40 MeV (!) (Müller *et al* 1983). This behaviour can be understood on the basis of direct ejection of electrons from outer or inner shells with subsequent relaxation processes. At sufficiently high energies, i.e. when the plane-wave Born approximation becomes valid, the distribution over energy transfers by the primary electron resembles the optical oscillator strength. Since the photoionisation cross section is highest near threshold in most cases slow outgoing electrons occur with high probability. Nevertheless, the rearrangement process subsequent to ionisation by a fast electron proceeds in a similar way to that following ionisation by an energetic photon, the reason being that even a slow outgoing electron hardly influences the rearrangement process except if its energy is less than a few eV.

In the present experiment the electron energies are limited by about 700 eV so that one cannot necessarily expect constant ratios $R_k^{(q)} = \sigma_{q,q+k}/\sigma_{q,q+1}$.

In figure 3 the measured ratios $R_k^{(q)}$ are shown as a function of the electron energy for $k=2$, $k=3$ and $k=4$ with the charge state of the ion Xe^{q+} as a parameter. While for double ionisation the ratios $R_2^{(1)}$ and $R_2^{(4)}$ are approximately constant with $R_2^{(1)} \simeq 0.3$ for electron energies $E \gtrsim 100$ eV and $R_2^{(4)} \simeq 0.2$ for $E \gtrsim 200$ eV all other ratios tend to increase further with increasing electron energy, although for example the ratio of double to single ionisation cross sections has already reached $R_2^{(2)} = 0.69$ for $E \simeq 700$ eV. Thus, figure 3 reveals two important results. (i) Multiple ionisation may become nearly as likely as single ionisation for complex many-electron systems, e.g. the investigated Xe^{q+} ions. (ii) The structures in the ratios $R_k^{(q)}$ when plotted as a function of the electron energy exhibit the influence of indirect ionisation processes.

There is one additional feature in the cross section ratios which should be discussed. For a fixed number $k=2$ or $k=3$ and electron energies beyond 200 eV the ratios $R_k^{(q)}$ go over a maximum when plotted as a function of the charge state q. This is especially also true for $R^{(q)} = \Sigma_k R_k^{(q)}$ which represents the ratio of the total multiple ionisation strength to the single ionisation strength. $R^{(q)}$ is plotted in figure 4 as a function of q for Xe^{q+} with $q=0, 1, 2, 3, 4$ for $E=700$ eV. The value for $q=0$ is taken from a publication by Nagy *et al* (1980). $R^{(q)}$ has a maximum at $q=2$ where it reaches about 80% and thus it is far higher than any value of $R^{(0)}$ ever observed for Xe atoms. The highest value for $R^{(0)}$ observed at 40 MeV electron energy is about 45% (Müller *et al* 1983). A possible reason for this behaviour may again be seen in the importance of indirect ionisation processes: The indirect ionisation processes involve inner shells. The cross sections for excitation or ionisation of inner shells can be assumed to be widely independent of the charge state q, i.e. the number of electrons missing in the outer shell, as long as q is not too large (see also Müller *et al* 1980). On the other hand the direct ejection of outer-shell electrons becomes more and more difficult with increasing q mostly because of the increase in the ionisation potential. Hence, the ratio of multiple and single ionisation may increase for small charge states q. These arguments are no longer valid for $q=4$ where we have previously found for Xe^{q+} ions that $\sigma_{4,5} > \sigma_{3,4}$ for electron energies beyond 200 eV (Achenbach *et al* 1984). There is also an increasing importance of indirect processes relevant to single ionisation which makes the ratio $R^{(q)}$ difficult to predict. More experimental and theoretical work is needed for a better understanding of the relative strength of multiple to single ionisation.

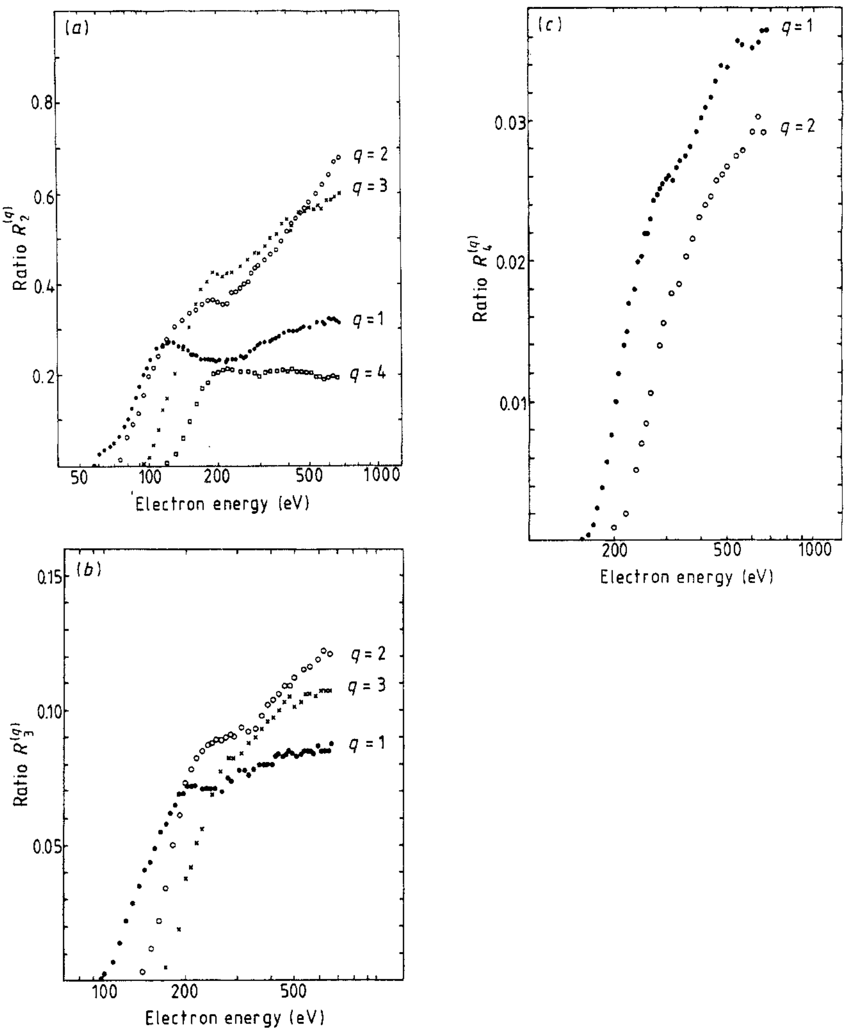

Figure 3. Relative strengths of double, threefold and fourfold ionisation against single ionisation. (a) Ratio $R_2^{(q)} = \sigma_{q,q+2}/\sigma_{q,q+1}$ with $q = 1, 2, 3, 4$. (b) Ratio $R_3^{(q)} = \sigma_{q,q+3}/\sigma_{q,q+1}$ with $q = 1, 2, 3$. (c) Ratio $R_4^{(q)} = \sigma_{q,q+4}/\sigma_{q,q+1}$ with $q = 1, 2$.

As a last point in this discussion we deal with the ratio $R_2^{(1)}$ for all ions for which direct cross section measurements have been published. As was already mentioned the ratios $R_k^{(q)}$ are expected to become constant for sufficiently high electron energy E. This trend can be seen in figure 5 where the ratios $R_2^{(1)}$ are shown as a function of E for Li^+, Ar^+, Rb^+, Xe^+ and Cs^+ ions. Figure 5 also reveals an increase of $R_2^{(1)}$ with increasing atomic number Z of the ion.

A very similar dependence has been observed for electron impact ionisation of the atoms He, Ne, Ar, Kr and Xe by Müller *et al* (1983) whose measurements are in good agreement with calculations of cross sections for multiple ionisation. These calculations are based on the assumption of direct single ionisation of the different atomic subshells including the possibility of shake-off processes and subsequent undisturbed decay of

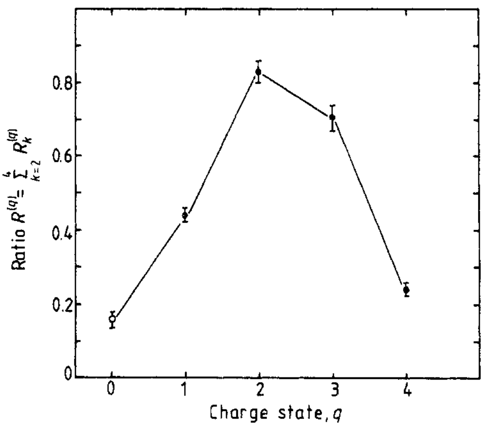

Figure 4. Relative strengths of multiple ionisation against single ionisation at $E_e = 700$ eV.

$$R^{(q)} = \sum_{k=2}^{4} R_k^{(q)} \text{ with } q = 0, 1, 2, 3, 4.$$

The value for $q = 0$ is taken from Nagy *et al* (1980).

the vacancies produced by electron or photon emission which may lead to multiple ionisation. While in the rare-gas series a monotonous increase of $R_2^{(0)}$ is found with increasing Z it is known from experiments with atoms from the first and second column of the periodic table that $R_2^{(0)}$ depends considerably on the shell structure of the atom to be ionised. For example the following ratios of double and single ionisation at 700 eV electron impact are found for neighbouring elements $R_2^{(0)} = 0.108$ for Xe (Nagy *et al* 1980), $R_2^{(0)} = 0.084$ for Cs (Tate and Smith 1934) and $R_2^{(0)} = 0.68$ for Ba (Dettmann and Karstensen 1982). The differences found in the Xe^{q+} series of figure 4 are of the same order and probably have similar reasons in the number of electrons outside a closed shell.

4. Conclusion

We have measured cross sections $\sigma_{q,q+k}$ for k-fold ionisation of Xe^{q+} ions by electron impact. Extremely large values of $\sigma_{q,q+k}$ have been found for multiple ionisation which seem to be due to a strong influence of indirect processes including ionisation and excitation of inner shells with subsequent autoionisation. In the case of double ionisation dominant contributions from 4d-shell ionisation–autoionisation have been identified for Xe^+ as well as for I^+. The ratios of multiple to single ionisation have been discussed in the framework of available crossed-beam data. The relative strengths of multiple versus single ionisation may increase with the charge state of the ion and nearly approach one for heavy ions ($Z = 54, 55$). Beside the fundamental interest in experiments of the present type an important practical consequence of our measurements has become obvious: multiple ionisation processes can *not* be neglected in respect to single ionisation when heavy atoms or ions are considered. The charge state balance of ions in a plasma is certainly influenced by multiple ionisation processes. Plasma modeling codes should therefore include both single and multiple ionisation cross sections.

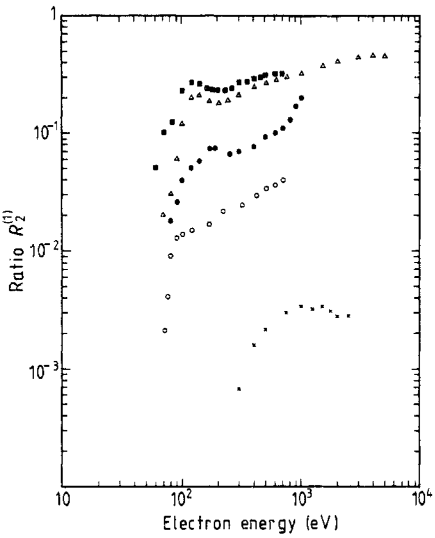

Figure 5. Relative strengths of double ionisation versus single ionisation for singly charged ions ($R_2^{(1)}$) for different ion species: Li^+ ($Z = 3$) (Peart and Dolder 1969) (×); Ar^+ ($Z = 18$) (Müller *et al* 1980) (○); Rb^+ ($Z = 37$) (Hughes and Feeney 1981) (●); Xe^+ ($Z = 54$) this work (■) and Cs^+ ($Z = 55$) (Hertling *et al* 1982) (△).

Acknowledgments

We would like to thank Mr W Schneider for technical assistance and skillful construction of apparatus. This work was supported in part by the Deutsche Forschungsgemeinschaft.

References

Achenbach C, Müller A, Salzborn E and Becker R 1983 *Phys. Rev. Lett.* **50** 2070–3
—— 1984 *J. Phys. B: At. Mol. Phys.* **17** 1405–25
Colestock P L, Connor K A, Hickok R L and Dandl R A 1978 *Phys. Rev. Lett.* **40** 1717–9
Cooper J W 1964 *Phys. Rev. Lett.* **13** 762–4
Defrance P, Claeys W and Brouillard F 1982 *J. Phys. B: At. Mol. Phys.* **15** 3509–16
Dettmann J M and Karstensen F 1982 *J. Phys. B: At. Mol. Phys.* **15** 287–300
Ederer D L 1964 *Phys. Rev. Lett.* **13** 760–2
El-Sherbini Th M, van der Wiel M J and de Heer F J 1970 *Physica* **48** 157–64
Gregory D C and Crandall D H 1983 *Phys. Rev.* A **27** 2338–41
Gregory D C, Dittner P F and Crandall D H 1983 *Phys. Rev.* A **27** 724–36
Gryzinski M 1965 *Phys. Rev.* A **138** 336–58
Halle J C, Lo H H and Fite W L 1981 *Phys. Rev.* A **23** 1708–16
Hertling D R, Feeney R K, Hughes D W and Sayle W E II 1982 *J. Appl. Phys.* **53** 5427–34
Hughes D W and Feeney R K 1981 *Phys. Rev.* A **23** 2241–9
Kieffer L J 1969 *At. Data* **1** 19–60
Kieffer L J and Dunn G H 1966 *Rev. Mod. Phys.* **38** 1–35
Lotz W 1968 *Z. Phys.* **216** 243–7
Lucatorto T B, McIlrath T J, Sugar J and Younger S M 1981 *Phys. Rev. Lett.* **47** 1124–8
Müller A and Frodl R 1980 *Phys. Rev. Lett.* **44** 29–32
Müller A, Groh W, Kneissl U, Heil R, Ströher H and Salzborn E 1983 *J. Phys. B: At. Mol. Phys.* **16** 2039–52

Müller A, Salzborn E, Frodl R, Becker R, Klein H and Winter H 1980 *J. Phys. B: At. Mol. Phys.* **13** 1877–99
Nagy P, Skutlartz A and Schmidt V 1980 *J. Phys. B: At. Mol. Phys.* **13** 1249–67
Peart B and Dolder K T 1969 *J. Phys. B: At. Mol. Phys.* **2** 1169–75
Peart B, Walton D S and Dolder K T 1971 *J. Phys. B: At. Mol. Phys.* **3** 1346–56
Pindzola M S, Griffin D C and Bottcher C 1983a *Phys. Rev.* A **27** 2331–7
—— 1983b *J. Phys. B: At. Mol. Phys.* **16** L355–60
Rinn K, Müller A, Eichenauer H and Salzborn E 1982 *Rev. Sci. Instrum.* **53** 829–37
Schram B L 1966 *Physica* **32** 197–208
Schram B L, Boerboom A J H and Kistemaker J 1966 *Physica* **32** 185–96
Sinz W 1981 *Nucl. Instrum. Meth.* **187** 259–62
Tate J T and Smith P T 1934 *Phys. Rev.* **46** 773–6
Younger S M 1980 *Phys. Rev.* A **22** 2682–9
—— 1982 *Phys. Rev.* A **26** 3177–86
Woodruff P R, Hublet M C and Harrison M F A 1978 *J. Phys. B: At. Mol. Phys.* **11** L305–8